SPINEL $LiFe_xCo_{2-X}O_4$ ($0.25 \leq x \leq 1$) AS CATHODES IN LITHIUM BATTERIES. RELATIONSHIP BETWEEN IONIC DISTRIBUTION AND LITHIUM ION INSERTION

*NICOLE MUCHNICK, FRANCISCO HERRERA, DANIELA ALBURQUENQUE, RUBEN PASTENE, JUAN ORTIZ, JUAN LUIS GAUTIER**

LEFS, Dpto. de Química de los Materiales, Facultad de Química y Biología, Universidad de Santiago de Chile, Av. L.B. O'Higgins 3363, 9170022 Santiago, Chile.

(Received: July 2, 2013 - Accepted: November 19, 2013)

ABSTRACT

Spinel $LiFe_xCo_{2-x}O4$ samples with $0.25 \leq x \leq 1$ were synthesized by the sol-gel Pechini method at 300ºC in order to study the impact on their structural and electrochemical properties due to the substitution of Co by Fe. The specific capacity for lithium insertion into the electrode materials depend on lithium diffusion coefficient DLi which in turn depends on the $Fe^{3+}/(Fe^{3+}+Co^{3+}+Co^{4+})$ octahedral cationic ratio.

Keywords: Lithium- Ferrites, spinels, diffusion coefficient, Li-ion batteries, sol-gel

1.INTRODUCTION

Li-ion batteries possess high energy density compared with Ni-Cd, NiMH, LiAl-FeS2 batteries, they are currently the most popular type of battery for portable electronic devices and they are growing in popularity for defense, automotive (EV,HEV,PHEV), storage systems using solar or wind powers and aerospace applications.

Recently published reviews about Li-ion batteries and lithium-air batteries [1-6] emphasize that the energy densities of the current lithium-ion batteries are limited mainly by the inherent low energy density of the available conventional cathode materials. Transition metal oxides consisting of highly oxidized redox couples ($Co^{3+/4+}$, $Ni^{3+/4+}$, $Mn^{3+/4+}$) have been studied as cathode materials, particularly LiCoO2, LiNiO2 and LiMn2O4. Besides, other transition metal oxides with layered and spinel structures, including polyanion based compounds, such as LiFePO4, have also been studied [7,8]. In these structures the lithium ions can easily be inserted reversibly during the insertion/extraction process. The ability of the cathode materials to intercalate Li-ions is closely related to its structure and both electrical and ionic conduction. Oxide spinels with different valence states of the metal ions, particularly M^{4+} ions, enhance the ionic conductivity by lowering the local Li^+ ion diffusion activation barriers [9]. In principle, it appears that the phase spinel, whose cubic structure ensures three dimensional diffusion paths, could deliver high power.

Spinel LiM2O4 is characterized as a close cubic packing (S.G. Fd 3m with 8 LiM2O4 units per unit cell), in which lithium ions are located at 8a tetrahedral sites, M ions at 16d octahedral sites, and oxygen ions at 32e sites. Since this unit cell has 64 tetrahedral and 32 octahedral holes, there are 56 empty tetrahedral and 16c empty octahedral sites. In spinel compounds it is well known that the lithium ions can be placed in 8a sites and in 16c sites, with the 16d sites being the empty ones. It has been shown that in the case of the Li1+xTi2O4 spinel the lithium insertion occurs in 16c sites for a wide range of x and the spinel becomes more stable. Whereas, when lithium moves from 8a sites to 16c, the process can take place only for the same x compositions [10]. Usually the charge/discharge process affects the capacity that can be measured during different constant discharge currents. It is well known that cell capacity decreases as the discharge current increases. A lower capacity higher discharge rate is related with high cell polarization [11].

The overall lithium insertion-extraction process involves the diffusion of Li+ ions from the anode towards the cathode surface, then a charge transfer process and solid-state diffusion of Li^+ into de cathode. The insertion-extraction process into host materials must occur with minimum structural modifications. On the other hand, there is an agreement within the battery community that lithium solid state diffusion is one of the key processes limiting the power of Li-ion batteries. The Li-ion diffusion coefficient determined in transition mixed oxide electrodes range from 10^{-12} to 10^{-8} cm^2s^{-1} depending on the technique used [12-18]. The Li-ion diffusion in spinels depends on the chemical composition and the degree of substitution by metals according to our recent report [19]. From a practical point of view, the spinel compound that has been the most studied is LiMn2O4 exhibiting lithium diffusion coefficient in the range $0.5 < DLi\ 10^{-9} < 4.9$ cm^2s^{-1} [20-22].

Literature reviwed had allowed to establish that the main trend in the battery research field is search an electrode materials which can introduce innovative reaction routes improvinge electrochemical properties, such as specific energy storage capacity, high current charge/discharge ability, cycle stability and high Li-ion diffusion coefficients [23-25]. However, little attention has been focalized to establish the relationships between the ionic oxide structural properties and its the electrochemical properties of spinel cathodes.

In this work, the lithium insertion process on the spinel LiFexCo2-xO4 ($0.25 \leq x \leq 1$) and its relationship with the cationic valence distribution in order to increase the knowledge about both the structural and the electrochemical parameters have been studied.

2.EXPERIMENTAL

The individual polycrystalline spinels of the LiFexCo2-xO4 series (x = 0.25, 0.5, 0.75 and 1) were synthesized via a modified Pechini method [26] at 300ºC, which involves the dissolution of the nitrate precursors of the respective metals in a 1:4 v/v mixture of 1 mol dm^{-3} of citric acid and ethylenglycol. Upon heating, esterification takes place (140ºC) and, after drying in vacuum at 190ºC, polymerization occurs with elimination of excess ethylenglycol. Upon gradually increasing the temperature at 2ºC mn^{-1} from 200ºC to 300ºC in an oxygen atmosphere, a polycrystalline and ultra fine powder (150 nm) was obtained after 48h of treatment. The products showed a brownish black colour. All the reagents, Fe (NO3)3 9H2O, Co (NO3)2 6H2O, LiNO3, ethylene glycol, citric acid, nitric acid, and hydrochloric acid were of analytical grade (Merck Chem. Co.) and were used without further purification. The metal cation concentrations were controlled by chemical analysis (AAS, Perkin Elmer 403) and inductive coupled plasma atomic emission spectrometry (ICP-AES). Sample quality was checked by the X-ray powder diffraction technique (XRD), using a Siemens D-5000 diffractometer at room temperature with CuKα (λ = 0.154056 nm) in Bragg-Brentano geometry, over the range $5 \leq 2q \leq 90$, with a sweep rate of 0.02º 2θ/step. The voltage and intensity current were set to 40 kV and 30 mA, respectively. The a-cell parameters, obtained using the Lattice program [27], were similar to those obtained using the Rietveld´s method [28]. The oxidation power was determined by chemical reduction of the oxide cations M^{n+} with $n \geq 3$ to n=2 using a VOSO4 sulfuric solution as soft reducing agent and standard KMnO4 solution to evaluate the excess of vanadyl sulfate. In order to corroborate the average cation valence and oxygen stoichiometry observed using VOSO4, an iodometric method that use KI and $K_2S_2O_3$ solutions was employed [29].

Transmission ^{57}Fe Mössbauer measurements were carried out at room temperature with a conventional spectrometer equipped with a ^{57}Co in an Rh matrix of 25mCi initial activity as γ- ray source. An Austin S-600 motor and an autonomous control system [30] were used in the constant acceleration mode to

e-mail: juan.gautier@usach.cl

vary the source velocity between ± 10 mms^{-1}. A pulse height analyzer was used to record signals, and the velocity distributions were folded and calibrated using the magnetic sextuplet spectrum of a high purity standard iron foil absorber (Wissel). Using the computer program "Recoil" [31] the velocity distributions were analyzed. We then obtained the isomer shift (δ), quadrupole splitting (Δ) and line width (Γ). The values of isomer shift were calibrated with respect to the centroid of the spectrum of α-Fe at RT. For the experiments, pellets of grounded solid samples were used. Low temperature Mössbauer spectroscopy was not available to us.

X-ray photoelectron spectroscopic (XPS) analyses were collected in an Escalab 2201-XL spectrometer under high vacuum (1×10^{-8} torr) using Mg Kα radiation (hv= 1253.6 eV). All the spectra were recorded at take off angles of 90°. XPS data analysis involved nonlinear background subtraction, and curve fitting using pseudo Voight line profiles. All binding energy (BE) values were charge-corrected to the C 1s signal which was set at BE = 284.6 eV. All the spectra were computer-fitted using a program based on procedures described in the literature [32]

The electrochemical measurements of the LiFexCo2-xO4 electrodes were performed in a Swagelock type cell [22] using oxide pellets (10 mm diameter, 1 mm thickness) prepared by pressing in a stainless steel grid, mixing 85wt% active oxides, 10wt% acetylene black as conductivity additive and 5wt% Teflon as mechanic additive. As anode and reference electrode a metallic Li-wire was used. The electrolyte was a 1M anhydrous LiPF6 solution in a 1:1(w/w) mixture of EC: DMC. The electrochemical cell was assembled in a globe box (Labconco) under an Ar-atmosphere. The studies of EIS were obtained using a 301 Voltalab PGZ Radiometer (Copenhagen). We have used an alternating perturbation of 200mV and a frequency (ω) between 10 kHz and 1 MHz. The galvanostatic lithium insertion was studied imposing a current of 42 μA during 60 min, then 15 min in open circuit and so on. The insertion curve was obtained from the open circuit potential to 1.7 V then the reaction was stopped.

3.RESULTS AND DISCUSSION

3.1Structural and Characterization.

The XRD spectra of the samples LiFexCo2-xO4 were indexed in the normal spinel cubic structure with Fd3m space group. Figure 1 is shown as example of the diffraction pattern of LiFe0.5 Co1.5O4. The locations and intensities of the main diffraction lines (111), (220), (311), (400) and (440) are almost the same for the other compositions.

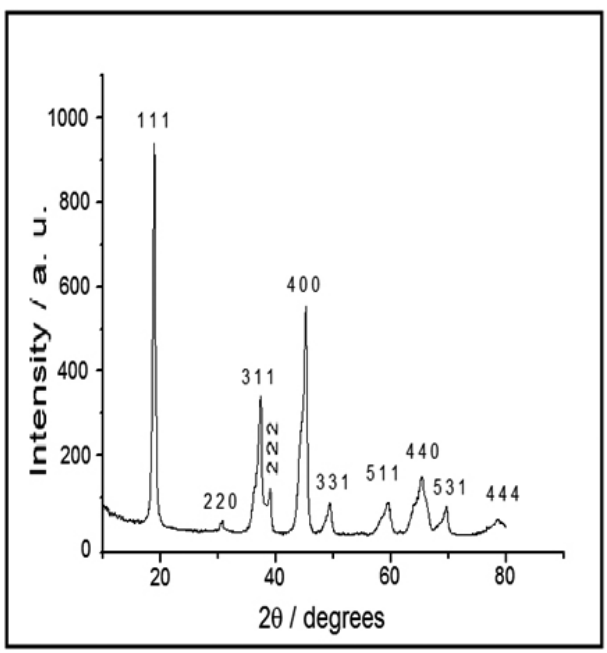

Fig 1. Diffraction pattern of $LiFe_{0.5}Co_{0.5}O_4$ oxide.

No extra diffraction lines were observed. It is relevant to remark that the intensity of the (111) line is related to the amount of lithium occupying the tetrahedral sites because all samples adopt the normal spinel structure. The wide diffraction peaks indicate low crystallinity. The lattice *a*-parameter increases with x in agreement with Fe^{3+} ions replacing Co^{3+} ions in octahedral sites in the spinel (Fig.2). The titration analysis was performed with the purpose to evaluate the oxygen content on each sample using the electrical charge. On the other hand, the a-cell parameter decreases to x = 0.5 and then increases with the inverse of cobalt concentration,$(Co^{3+}+Co^{4+})^{-1}$, showing the effect of Co^{4+} ions compensation (Fig 3)

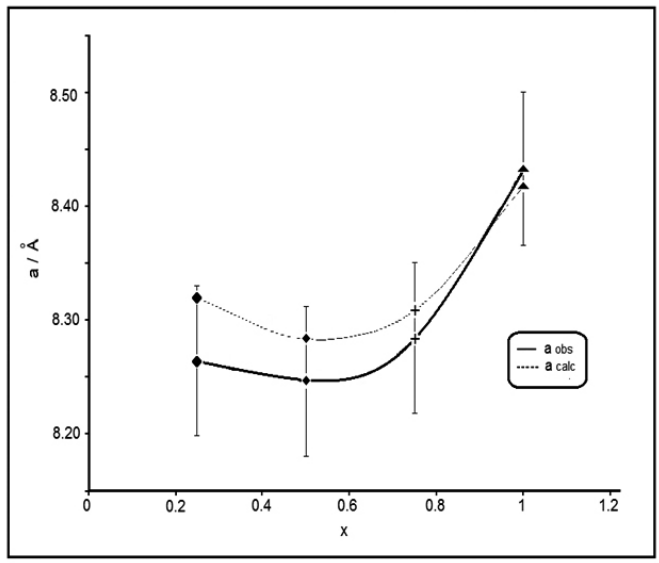

Fig 2. a-cell parameter (observed and calculated) vs. x.

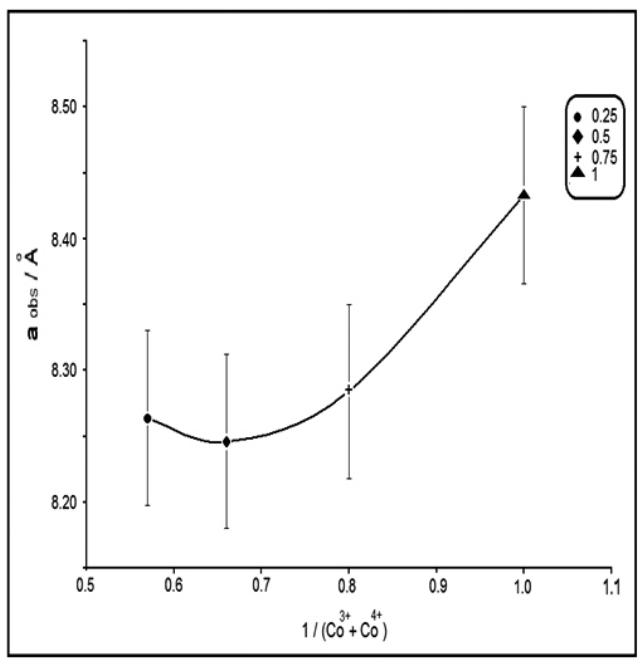

Fig 3. a-cell parameter vs. $(Co^{3+} + Co^{4+})^{-1}$ ratio.

From the formula LiFe**x**Co**2-x**O**4-v**, where v are vacancies, the oxygen stoichiometry (4-v) was 3.95; 4.03; 4.0; 3.56 for x = 0.25; 0.5; 0.75 and 1, respectively. From these values and considering the experimental errors, we have considering oxygen nonstoichiometry only for x=1, LiFeCoO3.6 □0.4.

RT Mössbauer spectra for the Fe-doped lithium cobaltite have shown the presence of a doublet for all cases (0.25≤ Fe ≤1.0) (Fig. 4). The Mössbauer parameters are show in Table 1. These values are indicative of the existence of high-spin Fe^{3+} ion in octahedral coordination, a feature which had already

been observed in spectra of compounds of related compositions, analyzed at room temperature [33-35].

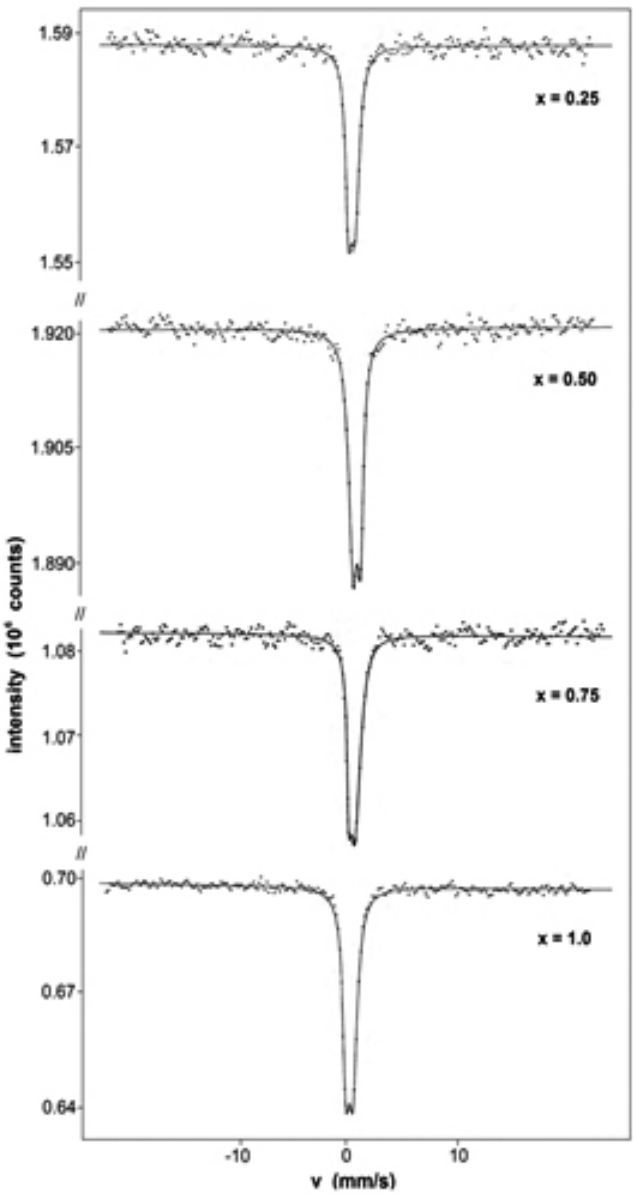

Fig. 4. Mössbauer spectra of the samples.

Table 1. ^{57}Fe Mössbauer hyperfine parameters of $LiFe_xCo_{2-x}O_4$ derived from the refined spectra shown in Figure 4.

x	δ / mm s^{-1}	D / mm s^{-1}	Γ / mm s^{-1}
0.25	0.339(24)	0.373(28)	0.248(24)
0.5	0.338(27)	0.388(25)	0.250(35)
0.75	0.318(62)	0.445(11)	0.267(12)
1.0	0.350(63)	0.391(11)	0.250(11)

Δ = isomer shift, D = splitting quadrupole, Γ = line width

The Fe 2p XPS spectra recorded for all samples were very similar (not shown) and indicated the presence of only the Fe^{3+} species (BE 2p**3/2** = 712.1-712.2 eV, 2p**1/2** = 725.6- 725.8eV, and a small shake up peak at 718.7eV) [36, 37]. In regards to the Co 2p signal, the XPS spectra have shown a doublet 2p**3/2** and 2p**1/2**. The first spin-orbit doublet, having a binding energy of the 2p**3/2** level of 779.1-780.6 eV and Δ = 2p**3/2** - 2p**1/2** splitting of 15.1eV, is characteristic of the octahedral Co^{3+} component, in agreement with our previous description for similar related oxides [38]. The peaks appearing at 780.3-780.5 eV with Δ splitting of 15.3 eV could be assigned to Co^{4+} as reported in the literature for mixed metal oxides [39, 40].

In order to propose the probable cationic distribution for each composition, several crystallographic distributions were formulated on the basis of experimental XRD, oxygen stoichiometry results, Mössbauer and XPS analysis and, considering the cations energetic preference to occupy tetrahedral and octahedral coordinations with the oxygen in the spinel [41], admitting the following ionic formula $Li^{+}[Fe^{3+}_{\mathbf{x}}Co^{3+}$ **(1-x+2v)** Co^{4+} **(1-2v)**$]O^{2-}$ **(4-v)**.

To validate the proposed distribution as a function of x, we have compared the experimental a-cell parameter value with the calculated a-cell parameter of the oxides on the basis of the cation-oxygen length in different sites of the spinel structure [42]. The following values were used [43] (Li+-O)**eg** = 1.97 Å, (Fe^{3+}-O)**t2g** = 2.045 Å, (Co^{3+}-O)**t2g** = 2.01 Å, (Co^{4+}-O)**t2g** = 1.93 Å. Table 2 shows the proposed distributions. A good agreement between the calculated cell parameter values and the observed ones was found, despite the errors of the measurements (see Fig 2).

For lithium insertion in mixed oxides, it is well known the fact that since the octahedral sites in spinels are the outermost sites of the structure, the reactivity increases due to the chemical nature of these sites. It is important then to study the effect of the octahedral cations on the physicochemical parameters of the Li-Fe-Co-O system, particularly in regards to their electrochemical behavior, i.e. specific capacity vs spinel structure. The calculated a-cell parameter and the observed presents a similar behavior with the cationic ratio Fe^{3+} / (Fe^{3+} + Co^{3+} + Co^{4+}), where x = 0.5 shows the minimum value (Fig.5).

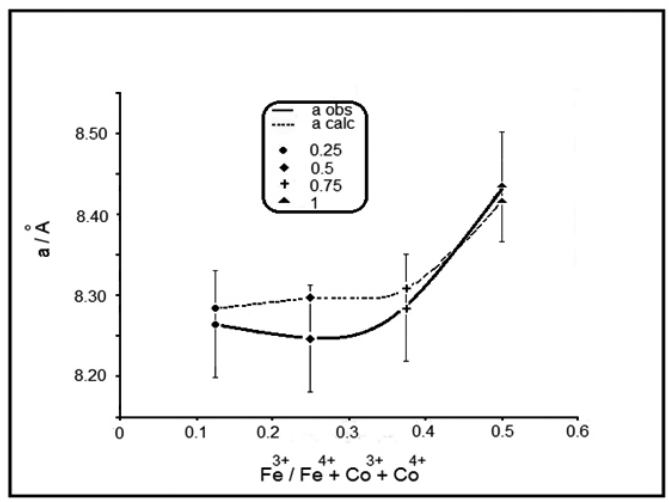

Fig 5. a-cell parameter (observed and calculated) vs. $Fe^{3+}/(Fe^{3+} + Co^{3+} + Co^{4+})$ ratio

3.2Lithium diffusion in the oxide network

To determine how easy it is to move the Li-ion from the surface to the inside of the oxide electrode, the diffusion coefficient D_{Li} must be measured. Fig. 6 shows the Nyquist diagrams as a function of the oxide composition determined using the EIS technique. It can be seen that in the case of x = 0.5, the charge region (Z') is remarkably more important (56 kWcm²) than for the other compositions, that are grouped below 23 kWcm². Whereas for the diffusion zone that is located in the linear part of the Warburg diagram corresponding to the low frequency region, it can be observed the existence of parallel straight lines. From the slope, s, of the straight lines of the Z**W** vs. $\omega^{-½}$ relationship (not shown), it was possible to determine D**Li** for each composition using the expression: σ = cst RT (nF) ²[√2/D½C**o**] where cst = RT(nF)= 25.393 10^{-3} AΩ, C**o** = 1M and F = 96485 [C/mol]. Table 3 shows these results. It can be observed that D**Li**

Table 2. Ionic distribution according to the formula $Li[Fe^{3+}_{x}Co^{3+}_{(1-x+2v)}Co^{4+}_{(1-v)}]O_{(4-v)}$ v = vacancies.

x	Li^+	Fe^{3+}	Co^{3+}	Co^{4+}	4-v/O	a_{cal}/Å	a_{obs}/Å
0.25	1	0.25	0.75	1	4	8.284	8.264± 0.01
0.5	1	0.5	0.5	1	4	8.296	8.246±0.069
0.75	1	0.75	0.25	1	4	8.308	8.284±0.079
1	1	1	0.88	0.12	3.6	8.417	8.433±0.107

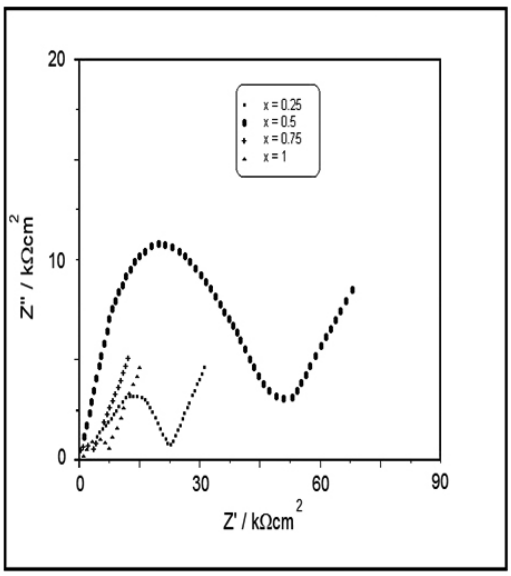

Fig 6. Nyquist diagrams vs. oxide composition

Table 3. Lithium diffusion coefficient vs. oxide composition x

x	0.25	0.5	0.75	1
D cm^2s^{-1}	$5.9\ 10^{-12}$	$4.0\ 10^{-18}$	$2.5\ 10^{-16}$	$4.3\ 10^{-14}$

depends on the Fe concentration replacing Co. In fact, the lithium diffusion coefficient decreases with x, showing a minimum for x = 0.5, and then increases (Fig 7).

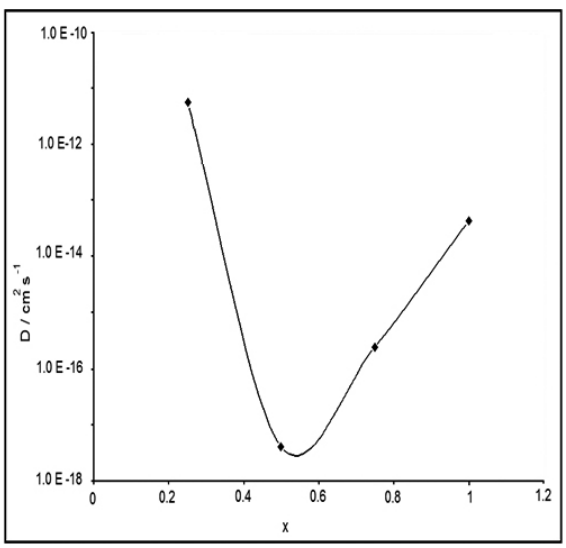

Fig 7. D vs. x

It is not possible to accept that the D**Li** depends only on the Co^{4+} ions because their concentration is constant. On the other hand, the concentration of Co^{3+} ions does not show a regular tendency (Fig 8). However, a similar curve is obtained when plotting D vs. $Fe^{3+}/(Fe^{3+} + Co^{3+} + Co^{4+})$ ratio showing the influence of Fe^{3+} ions which present the highest radius of the cations in the spinel (Fig 8).

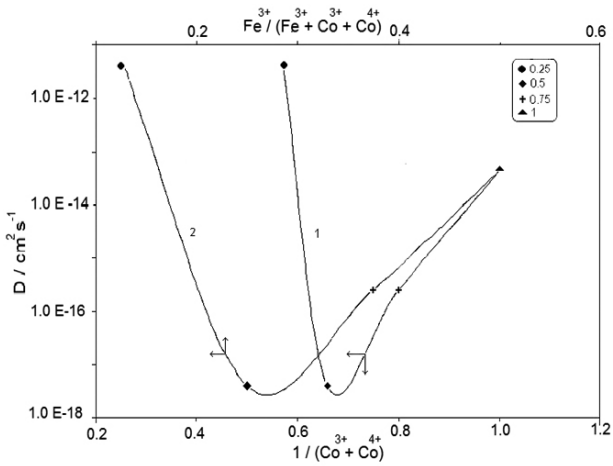

Fig 8. D vs. $Fe^{3+}/(Fe^{3+} + Co^{3+} + Co^{4+})$ ratio and D vs. $(Co^{3+} + Co^{4+})^{-1}$ ratio

3.3 Specific capacity versus concentration of octahedral cations.

In order to investigate rate capacity, the samples were discharged from open circuit voltage (Voc) to 1.7 V vs. Li/Li^+. The Voc decreases as a function of x, 1>0.75>0.5>0.25. As can be seen in the case of compositions x≥0.5, that the voltage decreases slowly until reaching 30 mAh/g, whereas for x = 0.25 it appears the lowest voltage plateau but the highest specific capacity measured at 2.3 V (Fig 9).

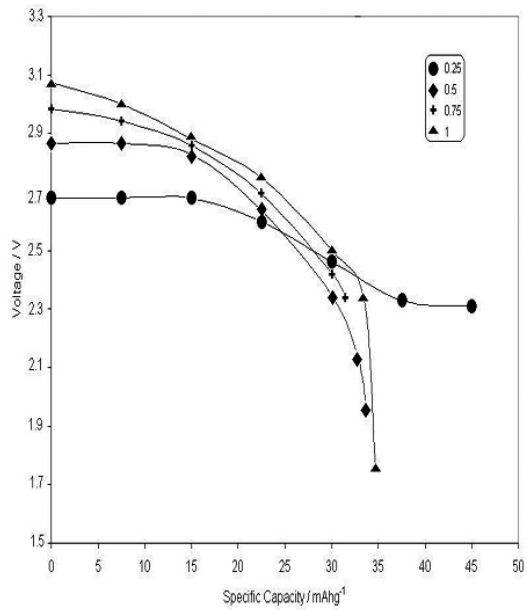

Fig 9. Discharge curves (5th cycle) vs. x (I = 42 mA

Regarding the Fig 10, it is clear that the specific capacity depends on x. It seems again that the octahedral cationic $Fe^{3+}/(Fe^{3+} + Co^{3+} + Co^{4+})$ ratio can explain the electrochemical reactivity shown by Fig. 11.

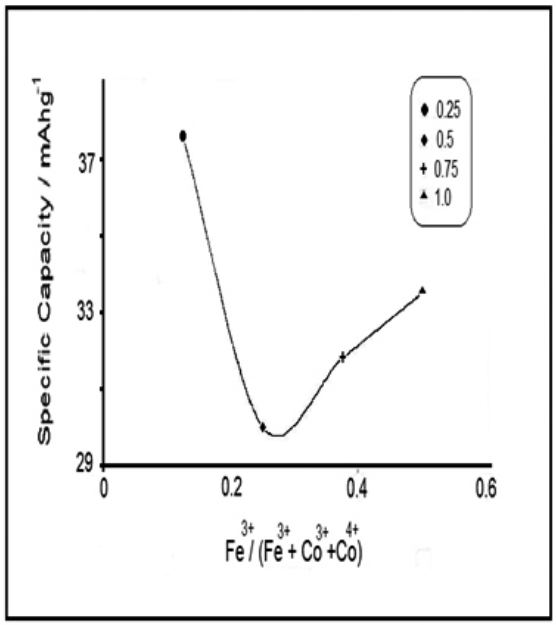

Fig 10. Specific capacity vs. x (I = 42μA)

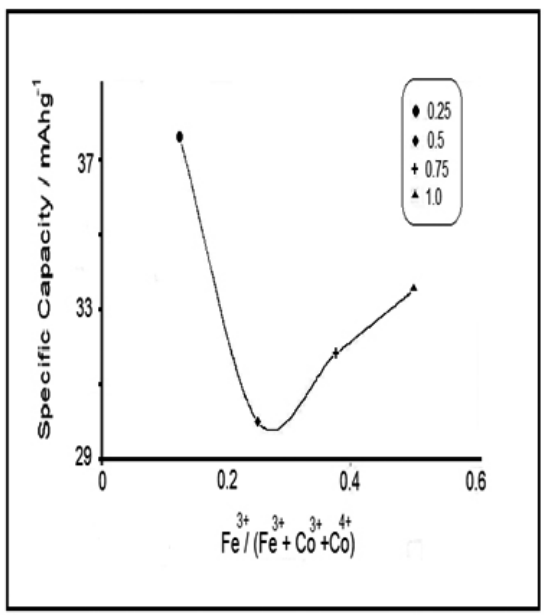

Fig 11. Specific capacity vs. $Fe^{3+}/(Fe^{3+} + Co^{3+} + Co^{4+})$ ratio

Indeed, the linear relationship obtained for the lithium diffusion coefficient D**Li** vs. specific capacity suggests that D**Li** is strongly correlated with the electrochemical reactivity. Again, the Co concentration (2-x) by itself cannot explain the tendency observed. Regarding Fig. 12, the maximum capacity and maximum D appear when x = 0.25 where the cationic ratio is the lowest (0.125). On the other hand, a minimal capacity is showed by x = 0.5 because the D has the lowest value of the oxide series (4×10^{-18} cm^2 s^{-1}) and the cationic ratio is lower than the other compositions. For the compositions x = 0.5, 0.75 and 1 both D and C increase as the cationic ratio increases.

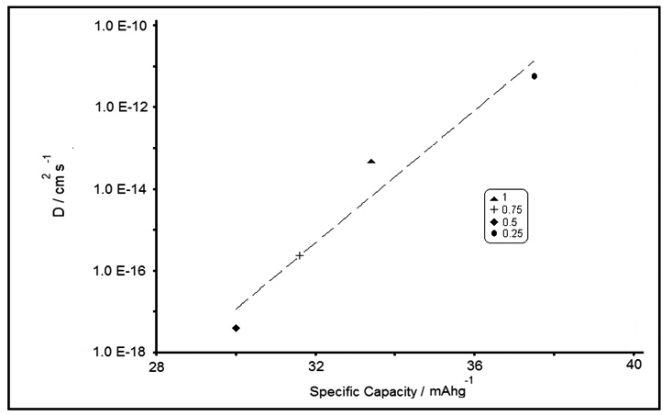

Fig 12. D vs. specific capacity

CONCLUSIONS

The present study shows that it is possible to synthesize stable phases having high oxidation states and exhibiting interesting physicochemical properties using a soft chemical procedure. The specific capacity of electrodes formed by lithium-iron cobaltites crystallizing in the spinel structure depends on the metal ions placed in octahedral sites of the spinel, particularly the $Fe^{3+}/(Fe^{3+}+Co^{3+}+Co^{4+})$ ratio which corresponds to half the concentration of cobalt substituted for iron. The diffusion coefficient of lithium DLi changes in a complicated way in the range of 10^{-12} to 10^{-18} cm^2s^{-1} under variations of the electrode composition. D**Li** depends simultaneously on the Co^{3+}, Co^{4+} and Fe^{3+} oxide concentrations.

ACKNOWLEDGMENTS

This work was supported by CONICYT, Grant Fondecyt 1110755. JO thanks Dicyt..

REFERENCES

1. B.Scrosati, J.Garche, J.Power Sources **195**, 2419, (2010)
2. J.B.Goodenough, Y.Kim, J.Power Sources **196**, 6688, (2011)
3. A.Kraytsberg, Y.E.Eli, J.Power Sources **196**, 886, (2011)
4. P.G.Bruce, S.A. Freunberger, L.J. Hardwich, J.M. Tarascon, Nature Mat. **11**, 19, (2012)
5. M-K-Songh, S.Park, F.M. Alamgir, J.Cho, M.Liu, Mat. Sc. Eng.R. **72,** 203, (2011)
6. D.Capsoni, M. Bini, S.Ferrari, E.Quartarone, P. Mustarelli, J.Power Sources **220**, 253, (2012)
7. J.W.Fergus, J.Power Sources **195**, 939, (2010)
8. H.Yang, S.Amiruddin, H.J.Bang, Y-K Sun, J.Prakast, J.Ind.Eng. Chem. **12,** 12, (2006)
9. B.Xu, S.Meng, J.Power Sources **195**, 4971, (2010)
10. M.Anicete-Santos, L.Gracia, A.Beltrán, J.Andrés, J.A.Varela, E.Longo, Physical Review B **77,** 85112, (2008)
11. M.Park, X.Zhang, M.Chung, G.B.Less, A.M. Sastry, J.Power Sources **195**, 7904,(2010)
12. Y.Zhu, Ch. Wang, J.Phys.Chem.C. **114**, 2830, (2010)
13. A.V.Churikov, V.O.Sycheva, Rus. J.Electrochem. **47,** 1043, (2011)
14. T.Uchida, Y.Morikawa, H.Ikuta, M.Wakihara, J. Electrochem. Soc. **143**, 2606, (1996)
15. .Takami, K.Hoshida, H.Inagaki, J.Electrochem. Soc. **158,** A725, (2011)
16. J.Bard, L.R.Faulkner, Electrochemical Methods Wiley Press: N.Y. 1980
17. C.Ho, I.D.Raistrick, R.A.Higgins, J.Electrochem. Soc.**127,** 345, (1980)
18. P.Bruce, G.A. Lisowska-Oleksisk, M.Y.Saidi, C.A.Vinvent, Solid State Ionics **57**, 353, (1992)
19. E. Meza, J.Ortiz, D. Ruiz- León, J.F. Marco, J.L.Gautier, Mat. Lett. **70**, 189, (2012)
20. D.Zhang, B.N.Popov, R.E.White, J.Electrochem. Soc. **147**, 831, (2000)
21. Y.Xia, H.Takeshige, H.Noguchi, M.Yoshio, J.Power Sources **56**, 61, (1995)
22. D.Guyomard, J.M.Tarascon, J.Electrochem. Soc. **139**, 937, (1992)
23. Ch.Jiang, E.Hosono, H.Zhou, Nanotoday 1, 28, (2006)

24. H.K.Liu, G.X.Wuan, Z.Guo, J.Wang, K.Konstantinov, J.Nanosc. Nanotech. **6**, 1, (2006)
25. A.M.Hasbem, R.S. El-Taweel, H.M. Abuzeid, A.E.Abdel-Ghany, A.E.Eid, H.Groult, A. Mauger, C.M.Julien, Ionics, **18**, 1, (2012)
26. M.P.Pechini, US: Pat. 3.330.697 (1967)
27. M.H.Mueller,L.Heaton, K.T.Miller, Acta Cryst. **13**, 828, (1960)
28. J.Rodriguez-Carvajal. ²Fullprof: a program for Rietveld refinement and pattern matching analysis², Laboratoire Leon Brillouin CEA-CNRS, Grenoble, France, 2007.
29. P.Barahona, V.Bodenez, T.Guizouarn, O.Peña, J. Ortiz, E.Ríos, R.Pastene, J.L. Gautier, J. Chil. Chem. Soc. **50**, 495, (2005)
30. A.A.Velásquez, J.M.Trujillo, A.L.Morales, J.E.Tobon, L.Reyes, J.R.Gancedo, Hyperf. Interac. **161**, 139, (2005)
31. K.Lagarec, D.G.Rancourt, RECOIL Mössbauer spectral analysis software for windows Dpt of Physics, University of Ottawa, version 1.0. 1998
32. P.M.A. Sherwood in : D. Briggs, MP Seah (Eds.) Practical Surface Analysis, 2nd edition Vol 1, Auger and X-ray Photoelectron Spectroscopy, Wiley, Chichester, 1990.
33. E.Ríos, Y.Y.Chen, M.Gracia, J.F.Marco, J.R.Gancedo, J.L.Gautier, Electrochim. Acta **47,** 559, (2001)
34. M.Gracia, J.F.Marco J.R.Gancedo, J.L.Gautier, E.Ríos, N.Menendez, J.Tornero, J.Mat. Chem. **13,** 844, (2003)
35. M.Gracia, J.F.Marco J.R.Gancedo, J.Ortiz, R.Pastene, J.L.Gautier, J.Phys. Chem. **114**, 12792, (2010)
36. D.Brion, App. Surf. Sci. **5**, 133, (1980)
37. J.F.Marco, M.Gracia, J.R.Gancedo, J.L.Gautier, F.J.Berry, Recent Res. Devel. Inorg. Organometallic Chem**. 1,** 45 (2001)
38. J.L.Gautier, E.Ríos, M.Gracia, J.F.Marco, J.R.Gancedo, Thin Solids Films **311,** 51, (1997)
39. B. Liu, Y.Zhang, L.Tang, Int. J. Hydrogen Energy **34**, 435, (2009)
40. W.Yang, J.Salim, S.Li, Ch.Sun, L.Chen, J.B.Goodenough, Y.Kim, J.Mat. Chem. **22**,18902,(2012)
41. A.Paul, S.Basu, Trans. J.Br.Ceram. Soc**. 73,**167, (1974)
42. P.Poix, Bull. Soc. Chim. Fr **5,**1085, (1965)
43. R.D.Shannon Acta Cryst. **A32**, 751, (1976)